This article has been accepted for publication in a future issue of this journal, but has not been fully edited. Content may change prior to final publication. Citation information: DOI 10.1109/TPWRD.2017.2711262, IEEE Transactions on Power Delivery

Accurate Two-Terminal Transmission Line Fault Location Using Traveling Waves

F. V. Lopes, *Member, IEEE,* K. M. Dantas, *Member, IEEE,* K. M. Silva, *Member, IEEE,* and F. B. Costa, *Member, IEEE*

***Abstract*—This paper presents an innovative two-terminal traveling wave (TW)-based fault location formulation. It depends only on the time difference between the first incident TW and the successive reflection from the fault point, at both line ends. Thereby, the proposed formulation requires neither data synchronization nor line parameters, which are sources of error that usually affect TW-based fault location schemes. Several faults on a typical 500 kV line were simulated to compare the proposed formulation performance with that of a classical two-end approach. The obtained results attest that the proposed formulation is able to accurately locate faults on transmission lines, even when data synchronism errors and uncertainties in the monitored line parameters exist.**

***Keywords*: Fault location, power systems, transmission lines, traveling waves, two-terminal unsynchronized data.**

I. Introduction

AIMING to speed up the restoration time of transmission lines after faults, researchers worldwide have made efforts to develop reliable and accurate fault location schemes. Hence, over the recent decades, several algorithms have been reported, among which those based on the theory of TWs have shown to be promising [1].

Among the TW-based fault location methods, those based on one- and two-end measurements are the most widespread [1]. These approaches have different advantages and disadvantages, so that the choice between one and the other is still difficult. The classical one-terminal method is independent of data synchronization, but it requires the detection of TWs reflected from the fault point [2], which is a task that has been reported for decades as not trivial to carry out [1]. On the other hand, although the classical two-terminal method requires only the detection of incident TWs at both line terminals, it depends on data synchronization [2], [3]. Furthermore, classical one- and two-terminal TW-based methods are inherently sensitive to inaccuracies in electrical line parameters, which are used to compute the TW propagation velocity [1].

In the literature on the subject, TW-based fault location algorithms which do not depend on data synchronization and/or TW propagation velocity have been reported. In [4], in addition to the incident TWs at both line ends, the first wavefront reflected from the fault point that reaches the reference terminal is detected, resulting in a two-end fault location formulation independent of the TW propagation velocity, i.e., electrical line parameters are not needed. However, despite of this advantage, data synchronization is still required. In [5] and [6], the two-end classical approach is adapted to be applied in real-time, considering the communication system latency effect. Both algorithms use the local fault locator clock as reference and synchronizes the remote data by compensating the communication channel latency. Still in [5], fault location solutions based on communication systems with large and negligible latency variability are also presented. By doing so, the need for an external common time reference such as the Global Positioning System (GPS) is eliminated [7], but the knowledge of the TW propagation velocity is still required. In [8], a two-terminal method which requires the detection of only incident ground and aerial mode TWs is presented. It neither uses information about the TW propagation velocity nor requires data synchronization, being advantageous over most existing two-terminal approaches. However, as aerial and ground mode TWs are analyzed, the algorithm application is limited to ground faults. In [9], an one-terminal method which requires neither the knowledge of the TW propagation velocity nor the two-end data synchronization is reported. Despite these advantages, it uses the time differences between the first incident TW and the second and third successive reflections from the fault point and remote terminal, so that its performance can be jeopardized if the reflection from the remote terminal is attenuated or when it does not exist, such as in three-phase permanent solid faults or when the line conductors break, preventing TWs reflected from the remote terminal from reaching the monitored bus.

Regarding the difficulties on the detection of wavefronts reflected from the fault point, two scenarios deserve special attention. In the first one, TWs reflected from the fault point need to be distinguished from those reflected from the remote line end. As typically occurs in ground faults, depending on the fault distance, TWs reflected from the remote terminal pass through the fault point toward the monitored bus and may reach it before the wavefront reflected back from the fault [3]. If so, fault location methods that require the detection of TWs reflected from the fault point may fail [1]. The second adverse scenario occurs due to adjacent or parallel lines connected to the monitored line. In both topologies, the problem lies in separating TWs reflected from the fault and those that come from other lines connected to the monitored terminals [9].

F. V. Lopes and K. M. Silva are with the Department of Electrical Engineering at University of Brasília (UnB), 70910-900 Brasília, Brazil. (e-mail: felipevlopes@unb.br, klebermelo@unb.br).

K. M. Dantas is with the Department of Electrical Engineering of Federal University of Campina Grande (UFCG) (e-mail: karcius@dee.ufcg.edu.br).

F. B. Costa is with the School of Science and Technology at Federal University of Rio Grande do Norte (UFRN), Natal 59.078-970, Brazil (e-mail: flaviocosta@ect.ufrn.br).

Manuscript received Month XX, 20XX; revised Month XX, 20XX.

0885-8977 (c) 2016 IEEE. Personal use is permitted, but republication/redistribution requires IEEE permission. See http://www.ieee.org/publications_standards/publications/rights/index.html for more information.

This article has been accepted for publication in a future issue of this journal, but has not been fully edited. Content may change prior to final publication. Citation information: DOI 10.1109/TPWRD.2017.2711262, IEEE Transactions on Power Delivery

In [10], voltage and current signals are used to separate incident and reflected wavefronts in a High-Voltage Direct Current (HVDC) system. Unfortunately, the analysis of voltage TWs in High-Voltage Alternating Current (HVAC) systems is usually avoided. Indeed, HVAC lines are normally equipped with coupling capacitor voltage transformers (CCVTs), which usually distort high frequency voltage components [11], making it difficult to analyze voltage TWs [12]. Therefore, in actual TW-based fault location schemes installed in AC systems, the use of current signals taken from current transformers (CTs) has been preferred [1], despite of difficulties to detect TWs reflected from the fault point.

In this work, an innovative two-terminal TW-based fault location formulation is proposed, which overcomes the aforementioned drawbacks. It computes the fault location from the time differences between the first incident TW and the successive reflection from the fault point at each line end, thereby the proposed formula requires neither an external common time reference nor TW propagation velocity, i.e., data synchronization and electrical line parameters are not needed. Such potentialities have not been found in existing TW-based fault location approaches, thereby the proposed solution may be advantageous for utilities during fault location procedures. Since TWs reflected from the fault point must be accurately detected, a fault location methodology is also proposed to overcome problems that may arise due to wavefronts reflected from other system terminals.

To demonstrate the proposed formulation advantages, several fault scenarios in a typical 500 kV/60 Hz line 200 km long were simulated, assuming different data synchronism errors and uncertainties in the monitored line electrical parameters. To evaluate the influence of adjacent lines on the proposed formulation, short lines connected at both terminals of the monitored line were also modeled. The obtained results indicate that the proposed fault location formula is accurate, even in power systems with no common time reference and significant uncertainties in line parameters.

II. Basic Concepts of TW-Based Fault Location Methods and Main Sources of Errors

The time-space diagram presented in Fig. 1 is used to illustrate the propagation of fault-induced TWs along a transmission line of length ℓ, which connects the line terminals where the fault location devices are installed: the local terminal (Bus i) and the remote terminal (Bus j). In order to explain the main sources of errors related to TW-based fault location algorithms, adjacent transmission lines connecting buses i_{adj} and j_{adj} to buses i and j, respectively, are taken into account. As illustrated in the diagram shown in Fig. 1: the fault is located at a distance d from Bus i; the first incident TWs reach buses i and j at the instants t_i and t_j, respectively; TWs reflected from the fault point arrive at buses i and j at t_{ir} and t_{jr}, respectively; TWs refracted at the fault point reach buses i and j at t_{it} and t_{jt}, respectively; TWs reflected back from buses i_{adj} and j_{adj} reach the monitored buses i and j at t_i^{adj} and t_j^{adj}, respectively.

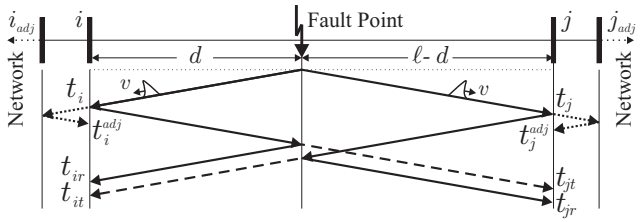

Fig. 1. Time-space diagram showing incident, reflected and refracted TWs as well as their arrival times at local and remote line terminals.

Assuming the Bus i as reference, the classical one-terminal TW-based method estimates the fault location using:

$$\widetilde{d} = 0.5(t_{ir} - t_i)v \ , \tag{1}$$

where $\widetilde{d}$ is the estimated fault location given in kilometers and v is the TW propagation velocity.

If both line ends are monitored, the two-terminal classical approach can be applied using:

$$\widetilde{d} = 0.5\left[\ell - (t_j - t_i)v\right] \ . \tag{2}$$

Ideally, if there are neither adjacent lines nor TWs refracted at the fault point traveling toward the monitored line ends, reliable fault location estimations are computed using (1), because t_i and t_{ir} (as well as t_j and t_{jr}, if Bus j is taken as reference) are easily detected. However, as depicted in Fig. 1, depending on the adjacent line length and on the fault distance, TWs reflected from adjacent buses may reach the monitored terminal before the wavefront reflected from the fault point, leading to errors in the fault location process. For instance, t_{ir} can be confused with t_i^{adj} or t_{it}, as well as t_{jr} with t_j^{adj} or t_{jt}, if Bus j is taken as reference (see Fig. 1). Facing this problem, the use of (2) seems to be a good solution, since it requires the identification of incident TWs only. Nevertheless, to properly compute the time period $(t_j - t_i)$, the clocks of both local and remote fault locators must be synchronized, imposing obstacles to the application of (2) in systems without a common time reference or when the time reference signal is lost [13]. Additionally, although the monitored line length can be experimentally estimated during line energization maneuvers [14], in the classical formulations (1) and (2), the propagation velocity is approximated to $v = 1/\sqrt{L_1 C_1}$, where L_1 and C_1 are the positive sequence line inductance and capacitance per unit of length, respectively [1]. Therefore, both one- and two-end approaches are subject to errors due to uncertainties in line electrical parameters.

III. Proposed Fault Location Formulation

The proposed fault location formulation is derived from the application of the classical one-terminal approach at both line ends. In order to present its principles, the time-space diagram illustrated in Fig. 1 is taken into account.

Assuming a precise detection at both line terminals of the first incident TWs and their successive reflections from the fault point, d and $\ell - d$ can be computed using:

$$d = 0.5\left(t_{ir} - t_i\right)v \ , \tag{3}$$

$$\ell - d = 0.5\left(t_{jr} - t_j\right)v \ . \tag{4}$$

0885-8977 (c) 2016 IEEE. Personal use is permitted, but republication/redistribution requires IEEE permission. See http://www.ieee.org/publications_standards/publications/rights/index.html for more information.

This article has been accepted for publication in a future issue of this journal, but has not been fully edited. Content may change prior to final publication. Citation information: DOI 10.1109/TPWRD.2017.2711262, IEEE Transactions on Power Delivery

Adding (3) and (4), the estimated line length $\widetilde{\ell}$ is computed:

$$\widetilde{\ell} = d + (\ell - d) = 0.5\left[(t_{ir} - t_i) + (t_{jr} - t_j)\right] v \ . \quad (5)$$

The fault distance estimation in per unit values $\widetilde{d}_{pu}$ can be estimated dividing (3) by (5), i.e., $\widetilde{d}_{pu} = d/\widetilde{\ell}$. Therefore, the proposed fault location formulation is derived as:

$$\widetilde{d}_{pu} = \frac{(t_{ir} - t_i)}{(t_{ir} - t_i) + (t_{jr} - t_j)} \ . \quad (6)$$

Analyzing (6), the following advantages are verified:

- As the time periods $(t_{ir} - t_i)$ and $(t_{jr} - t_j)$ are computed at each line end separately, data synchronization is not needed;
- Since v is not used in (6), the proposed formulation is independent of the electrical line parameters;
- The per unit fault distance estimation $\widetilde{d}_{pu}$ is not affected by line length inaccuracies;
- The proposed formulation properly works even when the faulted line conductors break;
- The fault location formula (6) can be implemented using only aerial mode quantities, thereby it is applicable to all fault types interchangeably.

If the fault distance in kilometers is of interest, the line length ℓ must be known to compute the estimation $\widetilde{d} = \widetilde{d}_{pu}\ell$. Although ℓ values are usually known by utilities, the total line length could present some error [1]. If so, an approximate TW propagation velocity can be used in (1) to estimate ℓ during the energization maneuver of the monitored line [14], reducing the influence of line length inaccuracies on the fault distance estimation given in kilometers.

At this point of the development, the main challenge of the proposed formulation becomes the correct identification of the first TWs reflected from the fault point, which reach buses i and j at t_{ir} and t_{jr}, respectively. As aforementioned, the detection of t_{ir} and t_{jr} may be difficult to carry out depending on the fault type and existence of adjacent lines. Hence, a fault location methodology which allows the reliable application of (6) is proposed. Fig. 2 depicts the flowchart of the proposed methodology, whose blocks are described next.

A. Step 1: Modal Transformation

During transmission line faults, aerial and ground modes are superimposed in phase quantities, making it difficult to analyze TWs reflected from the fault point. Aiming to facilitate the estimation of t_{ir} and t_{jr}, aerial and ground modes are separated by using modal transformations such as the Clarke, Wedephol and Karrenbauer ones [1]. In the proposed methodology, fault-induced TWs are extracted from aerial mode currents obtained by means of the Clarke's transformation [15].

B. Step 2: Detection of Incident TWs

In this step, fault-induced TWs are extracted from aerial mode currents. To do so, several techniques available in the literature can be used, such as those based on differentiator-smoother filters [16], Park's transformation [17], discrete wavelet transform [18], etc. It should be highlighted that

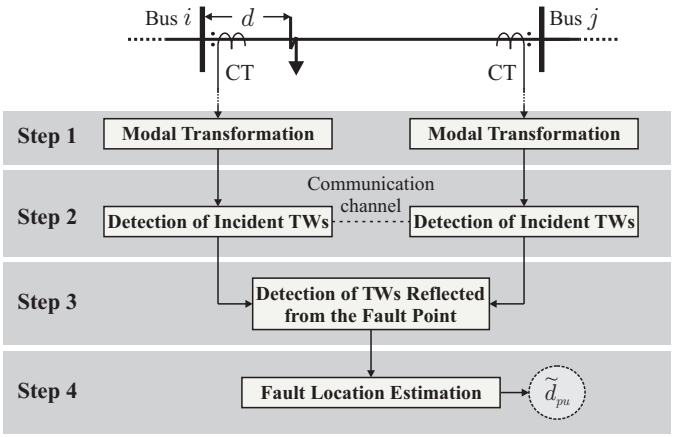

Fig. 2. Flowchart of the proposed methodology.

the goal of this paper is not to evaluate the performance of TW detectors, but rather, to demonstrate the advantages of the proposed fault location formulation. In this work, the differentiator-smoother filter was chosen to extract fault-induced TWs from the two-end measurements, since it has unity gain and can be applied in real-time, not requiring large computational burden [16].

In order to properly detect the first incident TWs on transmission lines, filtered signals are usually compared with thresholds. Basically, samples with magnitudes smaller than the predefined threshold are discarded, eliminating the electrical noise and system imbalance influence [19]. In this work, for the sake of simplicity, the threshold is adjusted as a percentage of the expected maximum fault-induced current TW amplitude measured at the line ends. The amplitude of a given measured current TW is the sum of the incident and reflected wavefronts, so that it depends on system and fault parameters, being calculated by [20], [21]:

$$I_{TW} = \frac{\sqrt{2} \cdot V_{SYS} \cdot \sin(\theta)}{Z_s + 2 \cdot R_F} \cdot \left(1 + \frac{Z_s - Z_T}{Z_s + Z_T}\right) \ , \quad (7)$$

where V_{SYS} is the RMS voltage magnitude at the fault point, θ is the fault inception angle, R_F is the fault resistance, Z_s is the line surge impedance and Z_T is the termination surge impedance behind the monitored terminal.

From (7), approximating V_{SYS} to the power system rated voltage, $Z_T = 0\ \Omega$ and $\theta = 90°$ are used to obtain the maximum expected incident current TW amplitude measured at the line terminals for a solid ground fault case:

$$I_{TW,max} = 2\sqrt{2} \cdot \left(\frac{V_{SYS}}{Z_s}\right) \ . \quad (8)$$

A threshold equal to 1% of $I_{TW,max}$ was used to test the proposed formulation. To compute $I_{TW,max}$, $Z_s = 233\ \Omega$ was considered, which is within the range of surge impedance values for typical 500 kV/60 Hz overhead lines [22]. Therefore, the incident TW is detected as soon as the absolute value of the filtered signal becomes higher than the threshold.

0885-8977 (c) 2016 IEEE. Personal use is permitted, but republication/redistribution requires IEEE permission. See http://www.ieee.org/publications_standards/publications/rights/index.html for more information.

This article has been accepted for publication in a future issue of this journal, but has not been fully edited. Content may change prior to final publication. Citation information: DOI 10.1109/TPWRD.2017.2711262, IEEE Transactions on Power Delivery

C. Step 3: Detection of TWs Reflected from the Fault Point

Aiming to permit a reliable identification of the arrival times at which the TWs reflected back from the fault point reach the line ends, auxiliary pre-estimations $\widetilde{m}$ of the fault distance are computed. From these pre-estimations, one can define bounds for search fields in time within which reflected TWs are expected to take place.

If synchronized records are available, pre-estimations $\widetilde{m}$ can be computed by means of the two-end classical formula (2). However, the proposed fault location formulation was developed to deal with unsynchronized data. Thus, in this work, the auxiliary pre-estimations are computed using the method reported in [5], which consists in the classical two-terminal TW-based fault location approach adapted to operate in real-time using two-end unsynchronized data. By compensating the communication system latency effect, the fault distance estimation $\widetilde{d}$ (in kilometers) is computed using [5]:

$$\widetilde{d} = 0.5\,[\ell - (\tau - \Gamma)\widetilde{v}] \ , \tag{9}$$

where τ is the absolute value of the time difference between the real-time detection of the first incident TWs at both line ends, Γ is the communication system latency and $\widetilde{v}$ is an approximate value of the TW propagation velocity. Actual fault locators usually consider $\widetilde{v}$ equal to 98% and 50% of the speed of light for overhead lines and underground cables, respectively [23]. Here, as an overhead 500 kV line is used to evaluate the proposed formulation, $\widetilde{v}$ equal to 98% of the speed of light is taken into account, but its setting for underground cables would be straightforward.

In practice, $\Gamma = \delta + \Delta\delta$ [24], being δ the intrinsic communication system latency and $\Delta\delta$ its variability. If dedicated fault locators are connected through dedicated communication channels, the data transmission latency has negligible variability [5], i.e., Γ is almost deterministic, being $\Delta\delta \approx 0$ and, consequently, $\Gamma \approx \delta$. As a result, Γ can be accurately estimated and compensated in the fault location formulation [25]. Based on that, if no common time reference is available, the use of dedicated devices and communication channels is indicated for the proposed fault location methodology, i.e., $\Gamma = \delta$ and δ is assumed to be known.

To create reliable search fields, pre-estimations $\widetilde{m}$ are computed considering different values of $\Delta\delta$ and $\widetilde{v}$. As a consequence, the search fields include a security margin which accommodate an eventual communication latency variability and possible deviations in the TW propagation times as well. To obtain $\widetilde{m}$ values, δ is assumed to be known and (9) is applied considering the combination of different values of $\Delta\delta$ and $\widetilde{v}$, resulting in:

$$\widetilde{m}(\Delta\delta_p,\widetilde{v}_p) = 0.5\,\{\ell - [\tau - (\delta + \Delta\delta_p)]\widetilde{v}_p\} \ , \tag{10}$$

where $\Delta\delta_p$ and $\widetilde{v}_p$ represent, respectively, the limit values of $\Delta\delta$ and $\widetilde{v}$ taken into account during the computation of the auxiliary pre-estimation $\widetilde{m}$ (note that $\Delta\delta_p \neq 0$ and $\widetilde{v}_p$ is not equal to $\widetilde{v}$ used in (9)).

In this work, $\widetilde{v}_p$ equal to 96% and 99% of the speed of light and $\Delta\delta_p$ equal to -2 μs and $+2$ μs are considered, resulting in four different $\widetilde{m}$ values. Therefore, being $\mathbf{M} = [\widetilde{m}_1,\widetilde{m}_2,\widetilde{m}_3,\widetilde{m}_4]$ the vector with the four auxiliary pre-estimations $\widetilde{m}$, at the reference terminal (Bus i), the left side limit $t_{inf,i}$ and the right side limit $t_{sup,i}$ of the proposed reflected TW local search field are finally defined as follows:

$$t_{inf,i} = t_i + (2/\bar{v}_{avg}) \cdot \min\left[\mathbf{M}\right] \ , \tag{11}$$

$$t_{sup,i} = t_i + (2/\bar{v}_{avg}) \cdot \max\left[\mathbf{M}\right] \ , \tag{12}$$

where $\bar{v}_{avg}$ is the average propagation velocity obtained from the $\widetilde{v}_p$ values considered in (10) and $\min[\cdot]$ and $\max[\cdot]$ are functions which return the minimum and maximum values of the input vector.

In order to obtain the search field at the remote terminal, i.e., $t_{inf,j}$ and $t_{sup,j}$, (11) and (12) are properly applied taking the Bus j as reference. Fig. 3 illustrates the search field created to find the TW reflected at the fault point during a solid AG short-circuit on a line 200 km long initiated at the phase A voltage peak. The fault is 50 km away from the monitored terminal and adjacent lines with length equal to 20 km are assumed to be connected to the monitored bus.

As shown in Fig. 3, the TW reflected from the fault point is in between other TWs, making it difficult to distinguish it from TWs reflected from other system terminals. Although two reflections from the adjacent line reach the monitored bus a few microseconds before the TW reflected from the fault, the proposed reflected TW search field properly restricts the region within which the TW reflected from the fault point takes place, resulting in the correct detection of the sought wavefront. Therefore, from the analysis of the two-end measurements, t_{ir} and t_{jr} are taken as the time instants at which the peak of the absolute value of the filtered signals inside the local and remote search fields are verified, respectively.

D. Step 4: Fault Location Estimation

In this step, a parabola-based interpolation technique is used to further improve the accuracy of the time instants t_i, t_j, t_{ir} and t_{jr} identified in steps 2 and 3. Three samples prior and following the peak of the measured incident and reflected current TWs (a total of seven samples of each wavefront) are taken into account to fit a parabola, whose maximum value is assumed to occur at the time instant at which the sought wavefronts reach the monitored terminal [12]. Then, using the refined values of t_i, t_j, t_{ir} and t_{jr}, the proposed fault location formula (6) is applied, resulting in the per unit fault location distance $\widetilde{d}_{pu}$, as illustrated in Fig. 2.

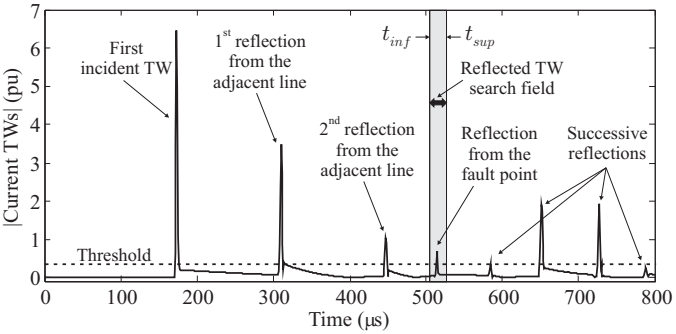

Fig. 3. Search field of the TW reflected from the fault point.

0885-8977 (c) 2016 IEEE. Personal use is permitted, but republication/redistribution requires IEEE permission. See http://www.ieee.org/publications_standards/publications/rights/index.html for more information.

This article has been accepted for publication in a future issue of this journal, but has not been fully edited. Content may change prior to final publication. Citation information: DOI 10.1109/TPWRD.2017.2711262, IEEE Transactions on Power Delivery

IV. Performance Evaluation

The proposed fault location methodology is evaluated through Alternative Transients Program (ATP) simulations of faults in the three-phase 500 kV/60 Hz power system shown in Fig. 4. It consists of a transmission line 200 km long, adjacent lines connected at buses i and j, whose lengths are represented by ℓ_1, ℓ_2, ℓ_3 and ℓ_4, and Thévenin circuits, which simulate the power systems around the monitored line. The electrical parameters of the modeled lines and Thévenin impedances were taken from the Brazilian power grid.

Aiming to analyze the errors of the proposed formulation itself, CTs at both line terminals were intentionally modeled as ideal instrument transformers. A sampling frequency equal to 1 MHz was simulated, so that secondary currents taken from the CTs were filtered using anti-aliasing second-order Butterworth filters with a cutoff frequency at 400 kHz.

In all simulations, the proposed fault location formulation and the classical two-terminal approach were applied, whose outputs will be represented hereafter by $\widetilde{d}_{prop}$ and $\widetilde{d}_{class}$, respectively. As the classical method depends on an external common time reference, a GPS signal to synchronize the two-end data was used. Also, the line length ℓ was assumed to be known, such that $\widetilde{d}_{prop}$ and $\widetilde{d}_{class}$ are given in kilometers. AG, AB, ABG and ABC faults were simulated, considering an inception angle equal to 90°. For each fault type, solid faults and faults with resistances equal to 50 Ω were analyzed. The fault distance d was varied from 20 km to 180 km with steps of 10 km and four different scenarios were evaluated: 1) ideal cases, considering exact line parameters and data synchronized via GPS; 2) line parameters with errors equal to ±10% of the actual values and data synchronized via GPS; 3) exact line parameters and GPS data synchronization error equal to 100 μs; and 4) simultaneous errors in line parameters (±10%) and in GPS data synchronization (100 μs).

Different values of ℓ_1, ℓ_2, ℓ_3 and ℓ_4 were also considered. Depending on the combination between the fault distance d and ℓ_1, ℓ_2, ℓ_3 and ℓ_4, wavefronts reflected from the adjacent buses and from the fault point may reach the monitored terminals at the same time or at very close instants. As a result, other TWs beyond those reflected from the fault point may take place inside the search fields defined in Step 3, what may lead to fault location errors. Therefore, to cover different possible situations that may exist in practical cases, the lengths ℓ_1, ℓ_2, ℓ_3 and ℓ_4 are adjusted considering: 1) adjacent lines with lengths submultiples of the simulated fault distances: ℓ_1 = 20 km, ℓ_2 = 50 km, ℓ_3 = 15 km and ℓ_4 = 35 km; and 2) adjacent lines with lengths that are not submultiples of the simulated fault distances: ℓ_1 = 23 km, ℓ_2 = 54 km, ℓ_3 = 17 km and ℓ_4 = 38 km. Combining all fault and system variables, 1632 different simulations were analyzed.

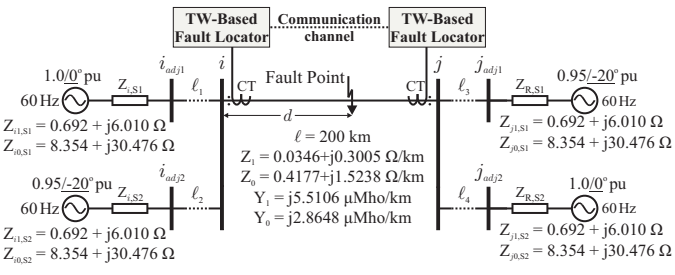

Fig. 4. Single-line diagram for the tested three-phase 500 kV power system.

A. Testing Results Considering Adjacent Lines with Lengths Submultiples of the Fault Distances

Fig. 5 depicts the cumulative frequency polygons obtained for $\widetilde{d}_{prop}$ and $\widetilde{d}_{class}$ absolute errors. These polygons plot the percentage of simulated faults against the maximum absolute fault location error [26]. In ideal cases, as shown in Fig. 5(a), $\widetilde{d}_{prop}$ and $\widetilde{d}_{class}$ proved to be reliable, resulting in errors smaller than 200 m. Notwithstanding, $\widetilde{d}_{prop}$ errors were smaller than $\widetilde{d}_{class}$ errors in about 97.1% of the simulated ideal cases. Meanwhile, when inaccuracies in line parameters and in the two-end data synchronism exist, $\widetilde{d}_{prop}$ remained more accurate than $\widetilde{d}_{class}$. Figs. 5(b), (c) and (d) show that the classical approach diverges (the cumulative frequency polygons computed for $\widetilde{d}_{class}$ do not reach 100% of faults in the scenarios 2, 3 and 4 in the range of errors shown in the figures), whereas, in all scenarios, $\widetilde{d}_{prop}$ resulted in errors that did not exceed 200 m in 100% of the simulations.

To highlight the advantages of the proposed formulation over the classical two-end approach, Fig. 6 presents scatter plots which show the $\widetilde{d}_{class}$ and $\widetilde{d}_{prop}$ absolute errors in the horizontal and vertical axes, respectively, for each studied scenario. In these plots, the light gray area (region at the bottom right) and dark gray area (region at the top left) are used to separate cases in which the proposed formulation accuracy has shown to be better or worse than the one of the two-terminal classical method, respectively.

Fig. 6 confirms that the proposed formulation is advantageous over the classical fault location approach. Among the evaluated cases, only in four fault cases in the scenario 1 (ideal cases), $\widetilde{d}_{prop}$ presented errors greater than those in $\widetilde{d}_{class}$. In these cases, TWs reflected from the adjacent buses arise inside the reflected TW search fields, reaching the monitored terminal at the same instant at which the TWs reflected from the fault point arrive, thereby the sought wavefront is distorted. However, even in these four cases, $\widetilde{d}_{prop}$ leads to errors up to 200 m (i.e., smaller than a typical tower span [7]), which are only 50 m greater than those of $\widetilde{d}_{class}$, revealing the proposed methodology reliability. In the remaining scenarios, for which inaccuracies in line parameters and data synchronization errors were taken into account, $\widetilde{d}_{prop}$ presented errors much smaller than those obtained by $\widetilde{d}_{class}$. As one can see in Figs. 6(b), (c) and (d), all points lies within the light gray region for the scenarios 2, 3 and 4, showing that $\widetilde{d}_{prop}$ has been more accurate than $\widetilde{d}_{class}$ in all simulations.

B. Testing Results Considering Adjacent Lines with Lengths that are not Submultiples of the Fault Distances

Fig. 7 presents the cumulative frequency polygons obtained for $\widetilde{d}_{prop}$ and $\widetilde{d}_{class}$ absolute errors. Again, both $\widetilde{d}_{prop}$ and $\widetilde{d}_{class}$ showed to be reliable in ideal cases. In fact, $\widetilde{d}_{prop}$ and $\widetilde{d}_{class}$ resulted in maximum errors up to 270 m. Even so, in

0885-8977 (c) 2016 IEEE. Personal use is permitted, but republication/redistribution requires IEEE permission. See http://www.ieee.org/publications_standards/publications/rights/index.html for more information.

This article has been accepted for publication in a future issue of this journal, but has not been fully edited. Content may change prior to final publication. Citation information: DOI 10.1109/TPWRD.2017.2711262, IEEE Transactions on Power Delivery

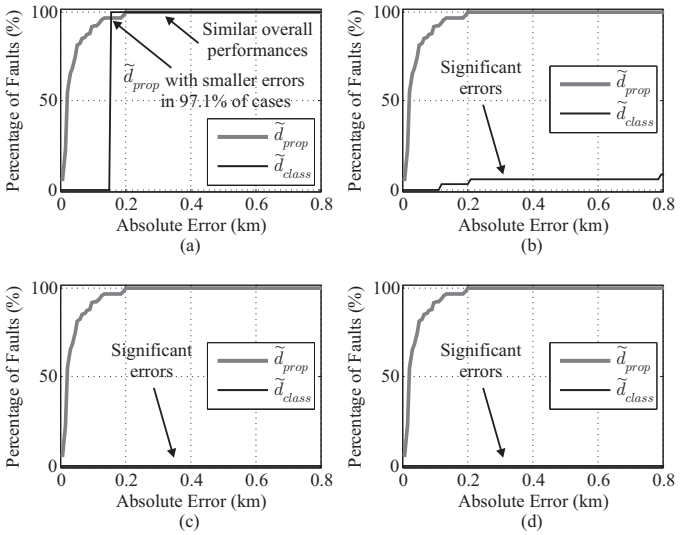

Fig. 5. Cumulative frequency polygons obtained considering adjacent lines with lengths that are submultiples of d in: (a) Scenario 1: Ideal cases; (b) Scenario 2: Errors in RLC parameters; (c) Scenario 3: Data synchronism errors; (d) Scenario 4: Errors in both RLC parameters and data synchronism.

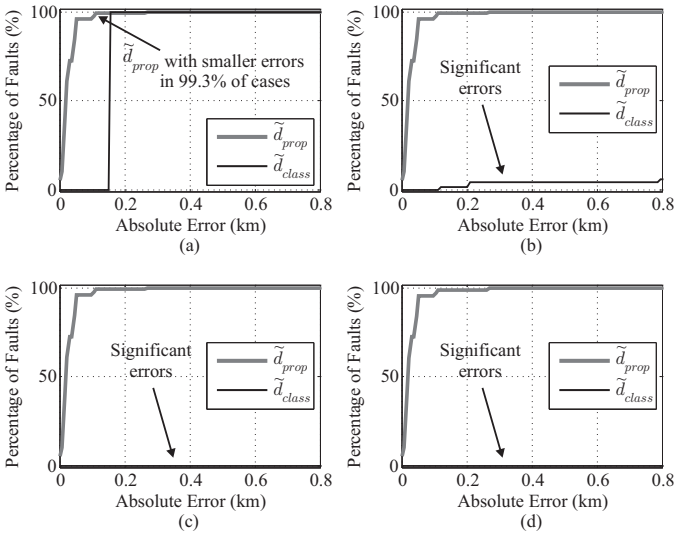

Fig. 7. Cumulative frequency polygons obtained considering adjacent lines with lengths that are not submultiples of d in: (a) Scenario 1: Ideal cases; (b) Scenario 2: Errors in RLC parameters; (c) Scenario 3: Data synchronism errors; (d) Scenario 4: Errors in both RLC parameters and data synchronism.

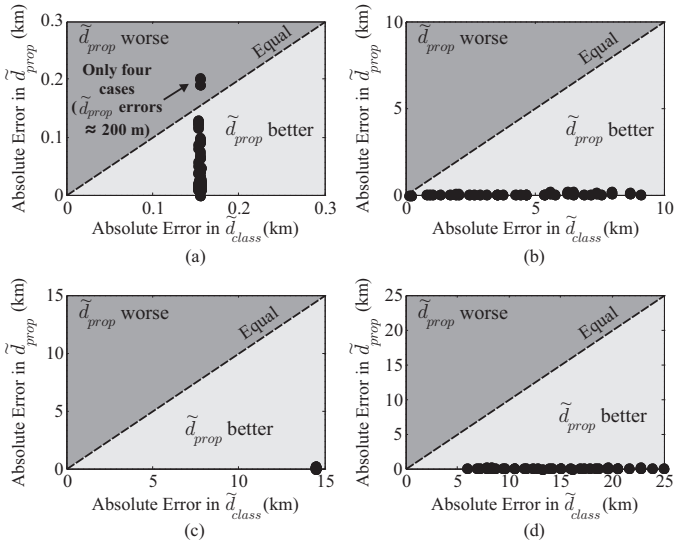

Fig. 6. Scatter plots of $\widetilde{d}_{class}$ and $\widetilde{d}_{prop}$ absolute errors considering adjacent lines with lengths that are submultiples of d in: (a) Scenario 1: Ideal cases; (b) Scenario 2: Errors in RLC parameters; (c) Scenario 3: Data synchronism errors; (d) Scenario 4: Errors in both RLC parameters and data synchronism.

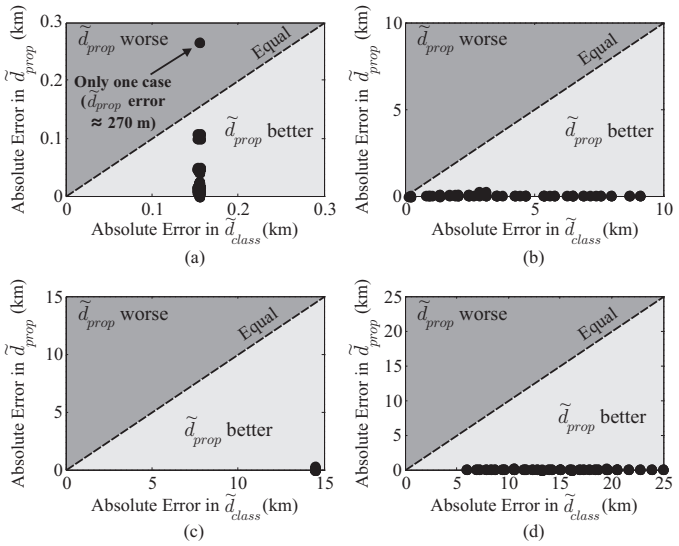

Fig. 8. Scatter plots of $\widetilde{d}_{class}$ and $\widetilde{d}_{prop}$ absolute errors considering adjacent lines with lengths that are not submultiples of d in: (a) Scenario 1: Ideal cases; (b) Scenario 2: Errors in RLC parameters; (c) Scenario 3: Data synchronism errors; (d) Scenario 4: Errors in both RLC parameters and data synchronism.

about 99.3% of the simulated ideal cases, $\widetilde{d}_{prop}$ presented errors smaller than those verified in $\widetilde{d}_{class}$ [Fig. 7(a)]. For this percentage of cases, $\widetilde{d}_{prop}$ errors did not exceed the order of 113 m. Furthermore, in the remaining scenarios, for which inaccuracies in line parameters and in data synchronism are considered, the proposed formulation has shown to be tremendously superior than the classical approach. As shown in Figs. 7(b), (c) and (d), the classical approach completely diverges, in such a way that the cumulative frequency polygon computed for $\widetilde{d}_{class}$ does not reach 100% of faults in the scenarios 2, 3 and 4 in the range of errors illustrated in the figures. On the other hand, $\widetilde{d}_{prop}$ remained as accurate as in the ideal case, presenting errors smaller than 113 m in 99.3% of the simulated faults and a maximum error equal to 270 m.

Fig. 8 presents scatter plots that relate $\widetilde{d}_{class}$ and $\widetilde{d}_{prop}$ absolute fault location errors for each studied fault scenario. Once more, as depicted in Fig. 8, the proposed formulation has shown to be advantageous over the classical approach. Indeed, it leads to errors much smaller than those obtained using the classical two-terminal method, even in the ideal scenario [Fig. 8(a)], for which the classical approach works properly. Only in one case the classical approach error was slightly smaller than the one obtained from the proposed formulation. In this case, wavefronts reflected from the adjacent buses take place inside the reflected TW search fields, reaching the monitored terminal at instants very close to that at which the TWs reflected from the fault point arrive. Nevertheless, since the reflected TW search fields used in the proposed methodology are narrow,

0885-8977 (c) 2016 IEEE. Personal use is permitted, but republication/redistribution requires IEEE permission. See http://www.ieee.org/publications_standards/publications/rights/index.html for more information.

This article has been accepted for publication in a future issue of this journal, but has not been fully edited. Content may change prior to final publication. Citation information: DOI 10.1109/TPWRD.2017.2711262, IEEE Transactions on Power Delivery

only a very small deviation was verified. In fact, the error difference between both classical and proposed approaches was of about 100 m only, attesting a reliable performance of the proposed methodology, even for the more adverse scenarios. Moreover, as illustrated in Figs. 8(b), (c) and (d), the errors in $\widetilde{d}_{prop}$ resulted in points inside the light gray region, presenting values approximately 20 times smaller than those in $\widetilde{d}_{class}$ in most cases.

Table I presents the averages and standard deviations of the absolute fault location errors computed for the estimations $\widetilde{d}_{class}$ and $\widetilde{d}_{prop}$, considering all the 1632 studied scenarios simultaneously. The obtained results show that the proposed fault location formulation presented overall errors much smaller than those of the classical two-terminal approach. The $\widetilde{d}_{prop}$ estimations presented an average fault location error equal to 31 m, whereas $\widetilde{d}_{class}$ values resulted in an average error of about 8.64 km. Furthermore, the standard deviation obtained from $\widetilde{d}_{prop}$ values was also much smaller than that computed for $\widetilde{d}_{class}$. Indeed, the $\widetilde{d}_{prop}$ estimations resulted in fault location errors with a standard deviation equal to 36 m, whereas $\widetilde{d}_{class}$ errors resulted in a standard deviation of about 6.94 km. It reveals that the proposed fault location methodology accommodates inaccuracies in transmission line parameters and data synchronism errors better than the classical two-terminal TW-based fault location approach.

TABLE I
AVERAGES AND STANDARD DEVIATIONS OF THE ABSOLUTE FAULT LOCATION ERRORS.

Analyzed Quantity	$\widetilde{d}_{class}$	$\widetilde{d}_{prop}$
Average (km)	8.643	0.031
Standard Deviation (km)	6.941	0.036

V. CONCLUSIONS

An innovative two-terminal TW-based fault location formulation was presented in this work. It neither requires the two-end data to be synchronized nor depends on the TW propagation velocity, i.e., it is independent of the electrical line parameters. To do so, the time difference between the arrival of the first incident fault-induced TW and the successive reflection from the fault point is computed at each line end separately, overcoming the need for a common time reference and eliminating the TW propagation velocity from the fault location formula. To properly apply the innovative formulation, a fault location methodology was also proposed.

The proposed formulation was evaluated by means of fault simulations carried out using the ATP. To analyze the main sources of errors which typically affect TW-based fault location schemes, a three-phase 500 kV/60 Hz test power system formed by a 200 km long transmission line with adjacent short lines was modeled. The influence of different lengths of the adjacent lines was also addressed. For each fault case, different scenarios were simulated, in which two-end data synchronism errors and inaccuracies in electrical line parameters were taken into account. From the combination of both fault and system variables, a total amount of 1632 different fault scenarios were analyzed.

The obtained results show that the proposed formulation is advantageous over the classical two-terminal approach, specially when there are significant uncertainties in electrical line parameters and in data synchronism. In all evaluated scenarios, the proposed fault location methodology has shown to be more accurate and reliable than the classical two-terminal method, resulting in errors smaller than 270 m even in the most adverse scenarios, in which data synchronism errors and inaccuracies in electrical line parameters are simultaneously taken into account. Considering all simulations, the proposed fault location methodology resulted in an average error of about 31 m with a standard deviation equal to 36 m, whereas the classical two-terminal approach diverged in some cases, resulting in an average error in the order of few kilometers. These results attest that the proposed formulation is accurate, reliable and suitable for transmission networks in which neither a common time reference nor the exact transmission line parameters are available.

ACKNOWLEDGMENT

The authors would like to thank the reviewers for their invaluable contributions.

VI. REFERENCES

[1] M. M. Saha, J. Izykowski, and E. Rosolowski, *Fault Location on Power Networks*, ser. Power Systems. London: Ed. Springer, 2010.

[2] P. F. Gale, P. Crossley, X. Bingyin, G. Yaozhong, B. Cory, and J. Barker, "Fault location based on travelling waves," in *5th International Conf. on Dev. in Power System Protection*, 1993, pp. 54–59.

[3] F. H. Magnago and A. Abur, "Fault location using wavelets," *IEEE Trans. on Power Delivery*, vol. 13, no. 4, pp. 1475–1480, Oct 1998.

[4] M. Gilany, D. k. Ibrahim, and E. S. T. Eldin, "Traveling-wave-based fault-location scheme for multiend-aged underground cable system," *IEEE Trans. on Power Delivery*, vol. 22, no. 1, pp. 82–89, Jan 2007.

[5] F. V. Lopes, K. M. Silva, F. B. Costa, W. L. A. Neves, and D. Fernandes, "Real-time traveling-wave-based fault location using two-terminal unsynchronized data," *IEEE Transactions on Power Delivery*, vol. 30, no. 3, pp. 1067–1076, June 2015.

[6] D. J. Marihart and N. W. Haagenson, "Automatic fault location for bonneville power administration," in *IEEE/PES Summer Meeting*, San Francisco, CA, July 1972.

[7] H. Lee and A. M. Mousa, "GPS travelling wave fault locator systems: investigation into the anomalous measurements related to lightning strikes," *IEEE Transactions on Power Delivery*, vol. 11, no. 3, pp. 1214–1223, Jul 1996.

[8] F. V. Lopes, "Settings-free traveling-wave-based earth fault location using unsynchronized two-terminal data," *IEEE Transactions on Power Delivery*, vol. 31, no. 5, pp. 2296–2298, Oct 2016.

[9] E. O. Schweitzer, A. Guzmán, M. V. Mynam, V. Skendzic, B. Kasztenny, C. Gallacher, and S. Marx, "Accurate single-end fault location and line-length estimation using traveling waves," in *13th International Conference on Developments in Power System Protection*, March 2016.

[10] M. Ando, E. Schweitzer, and R. A. Baker, "Development and field-data evaluation of single-end fault locator for two-terminal hvdv transmission lines-part 2 : Algorithm and evaluation," *IEEE Trans. on Power Apparatus and Systems*, vol. PAS-104, no. 12, pp. 3531–3537, Dec 1985.

[11] M. Kezunovic, L. Kojovic, V. Skendzic, C. W. Fromen, D. R. Sevcik, and S. L. Nilsson, "Digital models of coupling capacitor voltage transformers for protective relay transient studies," *IEEE Transactions on Power Delivery*, vol. 7, no. 4, pp. 1927–1935, Oct 1992.

[12] E. O. Schweitzer, A. Guzmán, M. V. Mynam, V. Skendzic, B. Kasztenny, and S. Marx, "Locating faults by the traveling waves they launch," in *50th Annual Minnesota Power Systems Conference*, November 2014.

[13] J. Izykowski, E. Rosolowski, P. Balcerek, M. Fulczyk, and M. Saha, "Accurate noniterative fault location algorithm utilizing two-end unsynchronized measurements," *IEEE Transactions on Power Delivery*, vol. 25, no. 1, pp. 72 –80, Jan. 2010.

0885-8977 (c) 2016 IEEE. Personal use is permitted, but republication/redistribution requires IEEE permission. See http://www.ieee.org/publications_standards/publications/rights/index.html for more information.

This article has been accepted for publication in a future issue of this journal, but has not been fully edited. Content may change prior to final publication. Citation information: DOI 10.1109/TPWRD.2017.2711262, IEEE Transactions on Power Delivery

[14] B. Kasztenny, A. Guzmán, N. Fischer, M. V. Mynam, and D. Taylor, "Practical setting considerations for protective relays that use incremental quantities and traveling waves," in *43rd Annual Western Protective Relay Conference*, Oct 2016.
[15] A. G. Phadke and J. S. Thorp, *Computer Relaying for Power Systems*, 2nd ed. New York, USA: John Wiley & Sons Inc, 2009.
[16] E. O. Schweitzer, B. Kasztenny, and M. V. Mynam, "Performance of time-domain line protection elements on real-world faults," in *42nd Annual Western Protective Relay Conference*, Oct. 2015.
[17] F. V. Lopes, D. Fernandes, and W. Neves, "A traveling-wave detection method based on Park's transformation for fault locators," *IEEE Transactions on Power Delivery*, vol. 28, no. 3, pp. 1626–1634, 2013.
[18] F. B. Costa, B. A. Souza, and N. S. D. Brito, "Real-time detection of fault-induced transients in transmission lines," *IET Electronics Letters*, pp. 753–755, May 2010.
[19] S. Santoso, E. Powers, W. Grady, and P. Hofmann, "Power quality assessment via wavelet transform analysis," *IEEE Transactions on Power Delivery*, vol. 11, no. 2, pp. 924 –930, apr 1996.
[20] A. Greenwood, *Electrical Transients in Power Systems*. New York, USA: 2nd Edition, John Wiley and Sons, 1991.
[21] A. Sharafi, M. Sanaye-Pasand, and P. Jafarian, "Ultra-high-speed protection of parallel transmission lines using current travelling waves," *IET Generation, Transmission Distribution*, vol. 5, no. 6, pp. 656–666, June 2011.
[22] J. D. Glover, M. S. Sarma, and T. J. Overbye, *Power System Analysis and Design*, 4th ed. CL - Engineering, 2009.
[23] S. L. Zimath, M. A. F. Ramos, and J. E. S. Filho, "Comparison of impedance and travelling wave fault location using real faults," in *2010 IEEE/PES Trans. and Dist. Conf. and Exposition*, April 2010, pp. 1 –5.
[24] H. J. Altuve and E. O. Schweitzer, *Modern Solutions for Protection, Control and Monitoring of Electric Power Systems*. Pullman, USA: Schweitzer Engineering Laboratories, Inc., 2010.
[25] H. Miller, J. Burger, N. Fischer, and B. Kasztenny, "Modern line current differential protection solutions," in *2010 63rd Annual Conference for Protective Relay Engineers*, 2010, pp. 1–25.
[26] J. F. Kenney and E. S. Keeping, *Mathematics of Statistics*. NJ: Van Nostrand: Princeton, 1962.

Felipe V. Lopes (M'10) was born in Brazil, 1985. He received his B.Sc., M.Sc. and Ph.D. degrees in Electrical Engineering from Federal University of Campina Grande (UFCG), Brazil, in 2009, 2011 and 2014, respectively. He is currently an Adjunct Professor at the Department of Electrical Engineering at the University of Brasília (UnB), Brazil. His research interests are electromagnetic transients, fault location, power system protection and real-time simulations.

Karcius M. Dantas (M'04) was born in Campina Grande, Brazil, in 1982. He received the B.Sc., M.Sc., and D.Sc. degrees in electrical engineering from Federal University of Campina Grande (UFCG), Campina Grande, Brazil, in 2005, 2007, and 2012, respectively. Since 2010, he has been with the Department of Electrical Engineering, UFCG. His research interests are electromagnetic transients in power systems and power quality.

Kleber M. Silva (M'05) was born in Brazil, 1980. He received his B.Sc., M.Sc. and Ph.D. degrees in Electrical Engineering from UFCG, Brazil, in 2004, 2005 and 2009, respectively. He is currently an Adjunct Professor at the Department of Electrical Engineering at the UnB, Brazil. His research interests are focused on electromagnetic transients and power system protection.

Flávio B. Costa (M'10) was born in Brazil, 1978. He received the B.Sc., M.Sc., and Ph.D. degrees in Electrical Engineering from UFCG, Brazil, in 2005, 2006, and 2010, respectively. Currently, he is a Professor at Federal University of Rio Grande do Norte (UFRN), Brazil. His research interests include power system protection, electric power quality, renewable energy systems, as well as smart-grid solutions.

0885-8977 (c) 2016 IEEE. Personal use is permitted, but republication/redistribution requires IEEE permission. See http://www.ieee.org/publications_standards/publications/rights/index.html for more information.